Spin-orbit coupling effects on the stability of two competing structures in Pb/Si(111) and Pb/Ge(111)

Xiao-Yan Ren,[1,2] Hyun-Jung Kim,[3] Seho Yi,[2] Yu Jia,[1,4,*] and Jun-Hyung Cho[2,1,†]

[1]*International Laboratory for Quantum Functional Materials of Henan, School of Physics and Engineering, Zhengzhou University, Zhengzhou 450001, China*

[2]*Department of Physics, Research Institute for Natural Sciences, Hanyang University, 17 Haengdang-Dong, Seongdong-Ku, Seoul 133-791, Korea*

[3]*Korea Institute for Advanced Study, 85 Hoegiro, Dongdaemun-gu, Seoul 130-722, Korea*

[4]*Key Laboratory for Special Functional Materials of Ministry of Education, School of Physics and Electronics, Henan University, Kaifeng 475004, China*

(Received 12 June 2016; published 24 August 2016)

Using first-principles density-functional theory (DFT) calculations with/without including the spin-orbit coupling (SOC), we systematically investigate the (4/3)-monolayer structure of Pb on the Si(111) or Ge(111) surface within the two competing structural models termed the H_3 and T_4 structures. We find that the SOC influences the relative stability of the two structures in both the Pb/Si(111) and the Pb/Ge(111) systems, i.e., our DFT calculation without including the SOC predicts that the T_4 structure is energetically favored over the H_3 structure by $\Delta E = 25$ meV for Pb/Si(111) and 22 meV for Pb/Ge(111), but the inclusion of SOC reverses their relative stability as $\Delta E = -12$ and -7 meV, respectively. Our analysis shows that the SOC-induced switching of the ground state is attributed to a more asymmetric surface charge distribution in the H_3 structure compared to the T_4 structure, which is associated with the hybridization of the Pb p_x, p_y, and p_z orbitals. This asymmetry of surface charge distribution gives rise to a relatively larger Rashba spin splitting of surface states as well as a relatively larger pseudogap opening in the H_3 structure. By the nudged elastic-band calculation, we obtain a sizable energy barrier from the H_3 to the T_4 structure as $\sim$0.59 and $\sim$0.27 eV for Pb/Si(111) and Pb/Ge(111), respectively. Based on the predicted thermodynamics and kinetics of Pb/Si(111) and Pb/Ge(111), we suggest not only the coexistence of the two energetically competing structures at low temperatures, but also the order-disorder transition at high temperatures.

DOI: 10.1103/PhysRevB.94.075436

I. INTRODUCTION

Two-dimensional (2D) electronic systems have attracted intensive attention due to their many exotic phenomena and potential applications in nanoelectronic devices [1–8]. Recently, metal-atom adsorption on semiconductor surfaces has been employed to generate spin-polarized current on the basis of the Rashba spin splitting where the spin-orbit coupling (SOC) lifts the spin degeneracy due to the broken inversion symmetry [9–16]. We here focus on the (4/3)-monolayer (ML) adsorption of Pb atoms on the Si(111) or Ge(111) surface, forming a dense phase with the $\sqrt{3} \times \sqrt{3}R30^\circ$ unit cell [see Figs. 1(a) and 1(b)]. It was recently reported [17] that this phase displays a large spin splitting of metallic surface bands on the semiconducting Ge(111) substrate, thereby promising for surface spin transport/accumulation because surface spin signals can be preserved over a long time within the substrate band gap.

Earlier reflection high-energy electron-diffraction, x-ray, and low-energy electron-diffraction measurements for Pb/Ge(111) suggested that the (4/3)-ML coverage has four Pb atoms per unit cell, three of which are located at off-centered T_1 sites and the fourth Pb atom at a H_3 site [18–20]. This structural model is termed the H_3 structure [see Fig. 1(a)], which preserves the C_{3v} symmetry. Recently, angle-resolved photoelectron spectroscopy (ARPES) and spin-resolved ARPES for Pb/Ge(111) demonstrated that a metallic surface-state band with a dominant Pb $6p$ character exhibits a large Rashba spin splitting of 200 meV [17]. This observed spin splitting of the surface state agreed well with the surface band structure of the H_3 structure (equivalently the close-packed structure), obtained using a density-functional theory (DFT) calculation with including the SOC [17,21]. However, earlier DFT calculations without SOC for Pb/Si(111) [22,23] and Pb/Ge(111) [24] predicted that the T_4 structure [see Fig. 1(b)] or the so-called chain structure with the broken C_{3v} symmetry is slightly more stable than the H_3 structure by less than a few tens of meV. This conflict of the ground state between experiments [18–20] and previous DFT calculations [22–24] may imply that the SOC influences the relative stability of the H_3 and T_4 structures in the Pb/Si(111) and Pb/Ge(111) surface systems. It is noted that a recent DFT + SOC calculation [17,21] for Pb/Ge(111) considered only the H_3 model for the (4/3)-ML-coverage structure. Therefore, it is very challenging to systematically examine the energetics of two energetically competing H_3 and T_4 structures for both Pb/Si(111) and Pb/Ge(111) systems by using the DFT calculations with/without including the SOC.

In the present study, we optimize the geometries of Pb/Si(111) and Pb/Ge(111) within the H_3 and T_4 structural models. Our DFT calculation without SOC demonstrates that the T_4 structure is energetically favored over the H_3 structure by $\Delta E = 25$ meV for Pb/Si(111) and 22 meV for Pb/Ge(111), consistent with previous DFT calculations [22–24]. However, the inclusion of SOC reverses their relative stability as $\Delta E = -12$ and -7 meV for Pb/Si(111) and

*Corresponding author: jiayu@zzu.edu.cn
†Corresponding author: chojh@hanyang.ac.kr

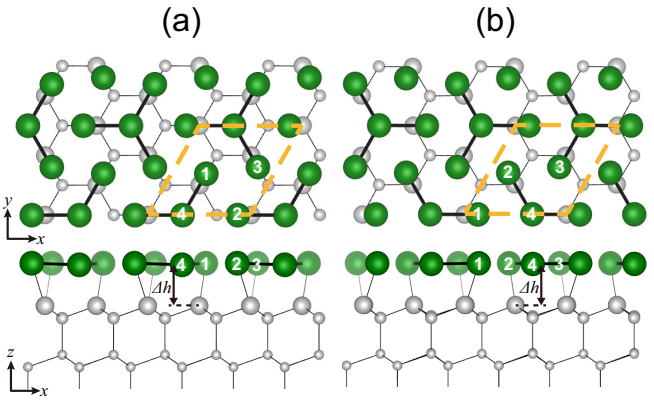

FIG. 1. Top and side views of the optimized (a) H_3 and (b) T_4 structures of Pb/Si(111). The green and gray circles represent Pb and Si atoms, respectively. For distinction, the Si atoms in the subsurface layers are drawn with small circles. The dashed line indicates the $\sqrt{3} \times \sqrt{3}R30^\circ$ unit cell where the four Pb atoms are numbered. The Pb_4 atom in (a) and (b) is located at the H_3 and T_4 sites, respectively. The **x**, **y**, and **z** axes point along the $[11\bar{2}]$, $[1\bar{1}0]$, and [111] directions, respectively. The height difference between the H_3 (T_4) Pb atom and the first Si-substrate layer is labeled as Δh.

Pb/Ge(111), respectively. We find that the H_3 structure has a more asymmetric surface charge distribution compared to the T_4 structure, which in turn results in a relatively larger Rashba spin splitting as well as a relatively larger pseudogap opening along the $\overline{KM}$ symmetry line. These results provide an explanation for the SOC-driven switching of the ground state. Moreover, our nudged elastic-band calculation obtains an energy barrier for the transition on going from the H_3 to the T_4 structure as large as $\sim$0.59 and $\sim$0.27 eV for Pb/Si(111) and Pb/Ge(111), respectively. Such a peculiar feature of the two competing structures separated by a sizable energy barrier in Pb/Si(111) and Pb/Ge(111) suggests not only the coexistence of the H_3 and T_4 phases at low temperatures, but also the order-disorder transition at high temperatures.

II. CALCULATIONAL METHODS

The present DFT calculations were performed using the Vienna *ab initio* simulation package with the projector-augmented-wave method and a plane-wave basis set [25,26]. For the treatment of exchange-correlation energy, we employed the generalized gradient approximation functional of Perdew-Burke-Ernzerhof [27]. The Pb/Si(111) and Pb/Ge(111) surfaces were modeled by a periodic slab geometry consisting of the 12 Si and Ge atomic layers with $\sim$25 Å of vacuum in between the slabs. The bottom of the Si or Ge substrate was passivated by one H atom. We employed a dipole correction that cancels the artificial electric field across the slab [28]. The kinetic-energy cutoff of the plane-wave basis set was taken to be 400 eV, and the **k**-space integration was performed with the 15 × 15 Monkhorst-Pack meshes in the surface Brillouin zones (SBZs) of the $\sqrt{3} \times \sqrt{3}R30^\circ$ unit cell. All atoms except the bottom two substrate layers were allowed to relax along the calculated forces until all the residual force components were less than 0.01 eV/Å.

TABLE I. Bond lengths (in Å) $d_{\text{Pb-Pb}}$ and $d_{\text{Pb-Si}}$ (or $d_{\text{Pb-Ge}}$) as well as Δh (see Fig. 1) in the H_3 and T_4 structures, obtained using DFT and DFT + SOC. Two different values of $d_{\text{Pb-Pb}}$ and $d'_{\text{Pb-Pb}}$ are given in the T_4 structure. The results for Pb/Ge(111) are given in parentheses.

		DFT	DFT + SOC
H_3	$d_{\text{Pb-Pb}}$	3.137 (3.224)	3.101 (3.188)
	$d_{\text{Pb}_1\text{-Si}}$	2.888 (2.893)	2.882 (2.897)
	$d_{\text{Pb}_2\text{-Si}}$	2.888 (2.893)	2.882 (2.897)
	$d_{\text{Pb}_3\text{-Si}}$	2.888 (2.893)	2.882 (2.897)
	Δh	2.596 (2.737)	2.649 (2.761)
T_4	$d_{\text{Pb-Pb}}$	3.183 (3.265)	3.133 (3.218)
	$d'_{\text{Pb-Pb}}$	3.193 (3.281)	3.142 (3.237)
	$d_{\text{Pb}_1\text{-Si}}$	2.877 (2.893)	2.867 (2.887)
	$d_{\text{Pb}_2\text{-Si}}$	2.882 (2.914)	2.871 (2.901)
	$d_{\text{Pb}_3\text{-Si}}$	2.882 (2.914)	2.871 (2.901)
	Δh	2.534 (2.537)	2.689 (2.672)

III. RESULTS

We begin to optimize the H_3 and T_4 structures of the Pb/Si(111) and Pb/Ge(111) surfaces using the DFT calculation in the absence of SOC. The optimized H_3 and T_4 structures of Pb/Si(111) are displayed in Figs. 1(a) and 1(b), respectively. We find that the T_4 structure is energetically more stable than the H_3 structure by $\Delta E = 25$ and 22 meV per $\sqrt{3} \times \sqrt{3}R30^\circ$ unit cell for Pb/Si(111) and Pb/Ge(111), respectively. This preference of the T_4 structure over the H_3 structure is consistent with previous DFT calculations [22–24]. The calculated bond lengths $d_{\text{Pb-Pb}}$ and $d_{\text{Pb-Si}}$ (or $d_{\text{Pb-Ge}}$) at the interface are given in Table I. It is noticeable that the H_3 structure of Pb/Si(111) [Pb/Ge(111)] has an equal value of $d_{\text{Pb-Pb}} = 3.137$ (3.224) Å between three nearest Pb-Pb atoms, thereby preserving the C_{3v} symmetry. Meanwhile, in the T_4 structure of Pb/Si(111) [Pb/Ge(111)], $d_{\text{Pb-Pb}} = 3.183$ (3.265) Å between two nearest Pb-Pb atoms is slightly shorter than the third one by $\sim$0.01 (0.02) Å, indicating the broken C_{3v} symmetry. This rotational symmetry breaking in the T_4 structure is also reflected by the position of the T_4 Pb adatom which is located at the off-centered T_4 site with a lateral displacement of $\sim$0.05 Å along the **x** direction [see Fig. 1(b)].

Figures 2(a) and 2(b) show the band structures of the H_3 and T_4 structural models of Pb/Si(111), respectively, obtained using the DFT calculation without SOC: For Pb/Ge(111), see Figs. 1S(a) and 1S(b) of the Supplemental Material [29]. The band projection onto the Pb p_x, p_y, and p_z orbitals is also displayed in Figs. 2(a) and 2(b). It is seen that the band structures of the H_3 and T_4 structures are very similar to each other. Especially, the band dispersion of the surface states crossing the Fermi level E_F is nearly parabolic along the $\overline{\Gamma M}$ and $\overline{\Gamma K}$ lines, indicating 2D electronic states in the Pb overlayer. As shown in Figs. 2(a) and 2(b), the orbital character of the surface states exhibits a strong **k** dependence along the symmetry lines. Consequently, the SOC may induce an efficient hybridization of the Pb p_x, p_y, and p_z orbitals as discussed below.

Next, we examine the SOC effects on the stability of the H_3 and T_4 structures using the DFT + SOC calculation. Interestingly, the inclusion of SOC changes the relative stability

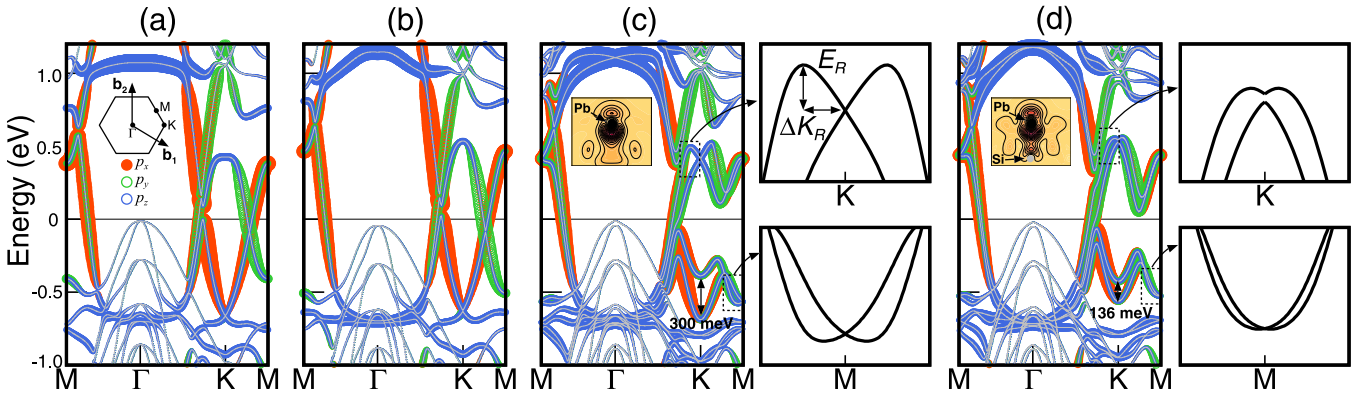

FIG. 2. Band structures of the (a) H_3 and (b) T_4 structural models, obtained using DFT. The corresponding ones obtained using DFT + SOC are given in (c) and (d), respectively. The bands projected onto the Pb p_x, p_y, and p_z orbitals are displayed with circles whose radii are proportional to the weights of such orbitals. The energy zero represents E_F. The inset in (a) shows the surface Brillouin zones of the $\sqrt{3} \times \sqrt{3}R30^\circ$ unit cell. In (c) and (d), the contour plots of the charge density of the lowest unoccupied surface state at the K point are drawn on the vertical plane containing the H_3 and T_4 Pb atoms, respectively, where the first line is at 0.3×10^{-3} electrons/Å^3 with spacings of 0.5×10^{-3} electrons/Å^3. A close-up of the spin splitting of the surface state at the K point (just above E_F) and the M point (just below E_F) is displayed for the H_3 and T_4 structures in (c) and (d), respectively, together with including their time-reversal counterparts.

of the two structures, i.e., the H_3 structure becomes more stable than the T_4 structure by 12 and 7 meV for Pb/Si(111) and Pb/Ge(111), respectively. As shown in Table I for the H_3 (T_4) structure of Pb/Si(111), the SOC decreases $d_{\text{Pb-Pb}}$ and $d_{\text{Pb-Si}}$ by $\sim$0.03 (0.05) and $\sim$0.01 (0.01) Å, respectively, but increases Δh by $\sim$0.05 (0.16) Å. On the other hand, for the H_3 (T_4) structure of Pb/Ge(111), the SOC produces decreases of $\sim$0.04 (0.05) and $\sim$0.01 (0.01) Å for $d_{\text{Pb-Pb}}$ and $d_{\text{Pb-Si}}$, respectively, and an increase of $\sim$0.03 (0.14) Å for Δh. To understand the SOC-induced switching of the ground state, we plot the band structures of the H_3 and T_4 models of Pb/Si(111) in Figs. 2(c) and 2(d), respectively, for Pb/Ge(111), see Figs. 1S(c) and 1S(d) of the Supplemental Material [29]. The spin degeneracy of surface states as well as other states is found to be lifted over the SBZ except at the high-symmetry points (i.e., Γ and M points). Specifically, it is seen that the H_3 structure has a spin splitting of 300 meV for the surface states at the K point just below E_F, larger than the corresponding one (136 meV) of the T_4 structure. The insets of Figs. 2(c) and 2(d) show a close-up of the spin splitting of the surface state at the K point along the $\overline{K\Gamma}$ direction (just above E_F) and the M point along the $\overline{MK}$ direction (just below E_F), obtained for the H_3 and T_4 structures, respectively. Obviously, these spin-split sub-bands illustrate the typical dispersion of the Rashba-type spin splitting. We fit the k-dependent dispersion of such spin-split sub-bands with the characteristic parameters, such as the momentum offset Δk_R and the Rashba energy E_R [see Fig. 2(c)] by using the Rashba spin-splitting eigenvalues $\varepsilon_\pm = \frac{\hbar^2 k^2}{2m^*} \pm \alpha_R k$, where m^* is the electron effective mass and α_R is the Rashba parameter. We find that the H_3 structure has $\alpha_R = 2.775$ (0.495) eV Å along $\overline{K\Gamma}$ ($\overline{MK}$), larger than 0.523 (0.093) eV Å for the T_4 structure. It is also noticeable that the H_3 structure exhibits a relatively larger pseudogap opening of 385 meV along the $\overline{KM}$ line compared to that (275 meV) of the T_4 structure: See Figs. 2(c) and 2(d). These relatively larger spin-splitting and pseudogap openings of the H_3 structure compared to the T_4 structure are caused by the hybridization of the Pb p_x, p_y, and p_z orbitals and the resulting asymmetry of surface charge distribution as discussed below, which lead to the SOC-induced switching of the ground state.

From the DFT + SOC calculation, the band projection of surface states shows a strong hybridization among the Pb p_x, p_y, and p_z orbitals [see Fig. 2(c) and 2(d)]. This SOC-induced hybridization is known to give not only a gap opening [30], but also an asymmetric surface charge distribution [16,31], which in turn determines the size of the Rashba spin splitting through the integral of the charge-density times the potential gradient along the direction perpendicular to the surface $\alpha_R \propto \int dV/dz\, \rho(\mathbf{r}) d\mathbf{r}$. As shown in the inset of Figs. 2(c) and 2(d), the H_3 structure has a more asymmetric charge character of the surface state compared to the T_4 structure, thereby giving rise to the above-mentioned relatively larger values of α_R. Indeed, a recent DFT calculation for the H_3 structure of Pb/Ge(111) reported that the observed large Rashba spin splitting is due to an asymmetric charge distribution in the vicinity of the H_3 Pb atom [21]. It is noteworthy that the SOC more dominantly changes the position of the T_4 Pb atom, which moves outward from the surface by $\sim$0.16 and $\sim$0.14 Å (see Table I) for Pb/Si(111) and Pb/Ge(111), respectively. This outward movement possibly contributes to the rather symmetric charge character of the surface state in the vicinity of the T_4 Pb atom as shown in the inset of Fig. 2(d).

Figures 3(a) and 3(b) show the helical spin textures of the H_3 and T_4 structures of Pb/Si(111) along the Fermi surface, respectively. It is seen that the spin angular momentum (SAM) direction rotates anticlockwise (clockwise) along the outer (inner) Fermi surface. The total spin-polarization $|\boldsymbol{S}| = \sqrt{S_x^2 + S_y^2 + S_z^2}$ and the longitudinal spin component S_z along the outer and inner Fermi surfaces are given in Figs. 3(c) and 3(d), respectively. We find that the value of $|\boldsymbol{S}|$ in the H_3 structure is slightly larger than that in the T_4 structure. It is also found that the magnitude of the transverse spin component S_x or S_y is larger in the H_3 structure compared to the T_4 structure, whereas that of S_z is reversed between the two structures. These different features between the two structures may be caused by

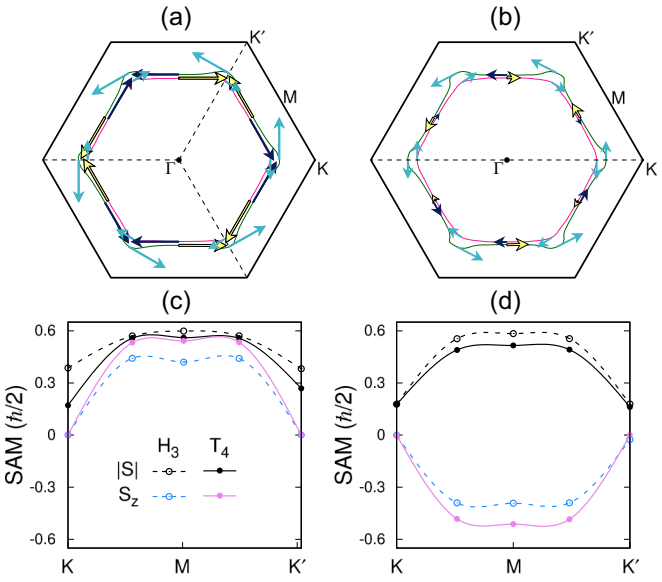

FIG. 3. Helical spin textures of the (a) H_3 and (b) T_4 structures of Pb/Si(111) along the Fermi surface. The SAM vectors with the negative, zero, and positive S_z components are represented with increasing brightness of the arrows. The total spin-polarization $|\boldsymbol{S}| = \sqrt{S_x^2 + S_y^2 + S_z^2}$ and the S_z component along the outer and inner Fermi surfaces are given in (c) and (d), respectively.

a relatively larger in-plane potential gradient in the T_4 structure due to its broken C_{3v} symmetry. As shown in Figs. 3(c) and 3(d), the spin vectors are highly polarized along the z direction, reflecting that the Pb overlayer on the Si(111) substrate has a large in-plane component of potential gradients. It is noted that the H_3 structure has the C_{3v} symmetry whereas the T_4 structure has one mirror-plane σ_v symmetry with the xz plane [see Fig. 1(b)]. Consequently, the whole spin textures along the Fermi surface satisfy the symmetries involved in the H_3 and T_4 structures, respectively [see Figs. 3(a) and 3(b)]. Since both H_3 and T_4 structures have a mirror symmetry of the xz plane, the S_x and S_z components change their signs, but the S_y component remains unchanged when the spin vectors within the irreducible part of the SBZ are reflected through the mirror plane along the Fermi surface. However, the spin vectors at the points crossing the $\overline{\Gamma K}$ line are oriented perpendicular to the mirror plane. Note that this mirror-plane symmetry is a combination of the proper rotation of 180° (about the y axis) with the inversion. Meanwhile, the whole spin textures shown in Figs. 3(a) and 3(b) also satisfy the time-reversal symmetry that simultaneously reverses the wave vector and spin.

To find the energy barrier for the phase transition between the H_3 and the T_4 structures, we calculate the energy profile along the transition path by using the nudged elastic-band method [32]. The calculated energy profile for the transition state (TS) is displayed in Fig. 4. We find that the TS is higher in energy than the H_3 structure, yielding an energy barrier of ∼0.59 (0.27) eV ongoing from the H_3 to the T_4 structure in Pb/Si(111) [Pb/Ge(111)]. The presence of a sizable energy barrier between the H_3 and the T_4 structures suggests that the two energetically competing structures can coexist in Pb/Si(111) or Pb/Ge(111) at low temperatures. However, as the temperature increases, thermal fluctuation between the two

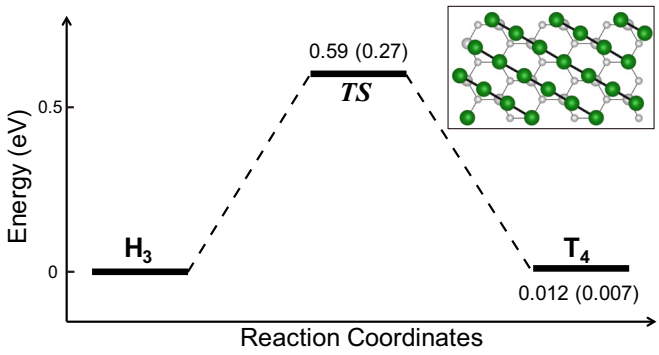

FIG. 4. Calculated energy profile along the transition pathway from the H_3 to the T_4 structure in Pb/Si(111). The atomic geometry of the TS is given. The numbers denote the total energies of TS and the T_4 structure relative to the H_3 structure. The corresponding energy values for Pb/Ge(111) are given in parentheses.

structures is plausible. Based on an Arrhenius-type activation process with the usual attempt frequency of $\sim 10^{13}$ Hz, we estimate the thermal fluctuation temperature as $\sim$ 270 and $\sim$ 125 K for Pb/Si(111) and Pb/Ge(111), respectively. This peculiar feature of the two competing structures separated by a sizable energy barrier is likely to cause not only the existence of complicated mixed phases at low temperatures, but also the order-disorder transition at high temperatures as observed in the Pb/Si(111) system [33,34].

IV. SUMMARY

We have investigated the (4/3)-ML Pb overlayer structures on the Si(111) and Ge(111) surfaces within the H_3 and T_4 models using the DFT calculations with/without including the SOC. For both Pb/Si(111) and Pb/Ge(111) systems, the DFT calculation without SOC showed that the T_4 structure is energetically favored over the H_3 structure, but the DFT + SOC calculation reverses their relative stability. This SOC-driven switching of the ground state is accounted for in terms of a more asymmetric surface charge distribution in the H_3 structure compared to the T_4 structure, which in turn gives rise to a relatively larger Rashba spin splitting as well as a relatively larger pseudogap opening along the $\overline{KM}$ line. In addition, our nudged elastic-band calculations for Pb/Si(111) and Pb/Ge(111) showed the presence of a sizable energy barrier between the H_3 and the T_4 structures so that the two energetically competing structures can coexist at low temperatures. Further experiments are needed for identifying such a close proximity of thermodynamically phase-separated ground states.

ACKNOWLEDGMENTS

This work was supported by a National Research Foundation of Korea (NRF) grant funded by the Korea Government (MSIP) (Grant No. 2015R1A2A2A01003248), by the National Basic Research Program of China (Grant No. 2012CB921300), the National Natural Science Foundation of China (Grant No. 11274280), and Innovation Scientists and Technicians Troop Construction Projects of Henan

Province. The calculations were performed by the KISTI supercomputing center through the strategic support program (Grant No. KSC-2015-C3-044) for the supercomputing application research.

[1] C. Brun, T. Cren, V. Cherkez, F. Debontridder, S. Pons, D. Fokin, M. C. Tringides, S. Bozhko, L. B. Ioffe, B. L. Altshuler, and D. Roditchev, Nat. Phys. **10**, 444 (2014).
[2] T. Zhang, P. Cheng, W.-J. Li, Y.-J. Sun, G. Wang, X.-G. Zhu, K. He, L. Wang, X. Ma, X. Chen, Y. Wang, Y. Liu, H.-Q. Lin, J.-F. Jia, and Q.-K. Xue, Nat. Phys. **6**, 104 (2010)
[3] Y. Kurosaki, Y. Shimizu, K. Miyagawa, K. Kanoda, and G. Saito, Phys. Rev. Lett. **95**, 177001 (2005).
[4] J. M. Carpinelli, H. H. Weitering, M. Bartkowiak, R. Stumpf, and E. W. Plummer, Phys. Rev. Lett. **79**, 2859 (1997).
[5] R. Coldea, D. A. Tennant, A. M. Tsvelik, and Z. Tylczynski, Phys. Rev. Lett. **86**, 1335 (2001).
[6] H. H. Weitering, J. M. Carpinelli, A. V. Melechko, J. Zhang, M. Bartkowiak, and E. W. Plummer, Science **285**, 2107 (1999).
[7] Z. Y. Meng, T. C. Lang, S. Wessel, F. F. Assaad, and A. Muramatsu, Nature (London) **464**, 847 (2010).
[8] Y. Shimizu, K. Miyagawa, K. Kanoda, M. Maesato, and G. Saito, Phys. Rev. Lett. **91**, 107001 (2003).
[9] A. V. Matetskiy, S. Ichinokura, L. V. Bondarenko, A. Y. Tupchaya, D. V. Gruznev, A. V. Zotov, A. A. Saranin, R. Hobara, A. Takayama, and S. Hasegawa, Phys. Rev. Lett. **115**, 147003 (2015).
[10] I. Barke, F. Zheng, T. K. Rügheimer, and F. J. Himpsel, Phys. Rev. Lett. **97**, 226405 (2006).
[11] I. Gierz, T. Suzuki, E. Frantzeskakis, S. Pons, S. Ostanin, A. Ernst, J. Henk, M. Grioni, K. Kern, and C. R. Ast, Phys. Rev. Lett. **103**, 046803 (2009).
[12] E. Frantzeskakis, S. Pons, and M. Grioni, Phys. Rev. B **82**, 085440 (2010).
[13] S. D. Stolwijk, A. B. Schmidt, M. Donath, K. Sakamoto, and P. Krüger, Phys. Rev. Lett. **111**, 176402 (2013).
[14] D. V. Gruznev, L. V. Bondarenko, A. V. Matetskiy, A. Y. Tupchaya, A. A. Alekseev, C. R. Hsing, C. M. Wei, S. V. Eremeev, A. V. Zotov, and A. A. Saranin, Phys. Rev. B **91**, 035421 (2015).
[15] S. D. Stolwijk, K. Sakamoto, A. B. Schmidt, P. Krüger, and M. Donath, Phys. Rev. B **90**, 161109 (2014).
[16] H.-J. Kim and J.-H. Cho, Phys. Rev. B **92**, 085303 (2015).
[17] K. Yaji, Y. Ohtsubo, S. Hatta, H. Okuyama, K. Miyamoto, T. Okuda, A. Kimura, H. Namatame, M. Taniguchi, and T. Aruga, Nat. Commun. **1**, 17 (2010).
[18] B. N. Dev, F. Grey, R. L. Johnson, and G. Materlik, Europhys. Lett. **6**, 311 (1988).
[19] R. Feidenhans'l, J. S. Pedersen, M. Nielsen, F. Grey, and R. L. Johnson, Surf. Sci. **178**, 927 (1986).
[20] H. Huang, C. M. Wei, H. Li, B. P. Tonner, and S. Y. Tong, Phys. Rev. Lett. **62**, 559 (1989).
[21] K. Yaji, S. Hatta, T. Aruga, and H. Okuyama, Phys. Rev. B **86**, 235317 (2012).
[22] T.-L. Chan, C. Z. Wang, M. Hupalo, M. C. Tringides, Z.-Y. Lu, and K. M. Ho, Phys. Rev. B **68**, 045410 (2003).
[23] M. Hupalo, T. L. Chan, C. Z. Wang, K. M. Ho, and M. C. Tringides, Phys. Rev. B **66**, 161410 (2002).
[24] F. Ancilotto, A. Selloni, and R. Car, Phys. Rev. Lett. **71**, 3685 (1993).
[25] G. Kresse and J. Hafner, Phys. Rev. B **48**, 13115 (1993).
[26] G. Kresse and J. Furthmüller, Comput. Mater. Sci. **6**, 15 (1996).
[27] J. P. Perdew, K. Burke, and M. Ernzerhof, Phys. Rev. Lett. **77**, 3865 (1996); **78**, 1396 (1997).
[28] J. Neugebauer and M. Scheffler, Phys. Rev. B **46**, 16067 (1992).
[29] See Supplemental Material at http://link.aps.org/supplemental/10.1103/PhysRevB.94.075436 for the band structures of the Pb/Ge(111) surface, obtained using DFT and DFT + SOC.
[30] S.-W. Kim, C. Liu, H.-J. Kim, J.-H. Lee, Y. Yao, K.-M. Ho, and J.-H. Cho, Phys. Rev. Lett. **115**, 096401 (2015).
[31] M. Nagano, A. Kodama, T. Shishidou, and T. Oguchi, J. Phys.: Condens. Matter **21**, 064239 (2009).
[32] G. Henkelman, B. P. Uberuaga, and H. Jónsson, J. Chem. Phys. **113**, 9901 (2000).
[33] K. Horikoshi, X. Tong, T. Nagao, and S. Hasegawa, Phys. Rev. B **60**, 13287 (1999).
[34] S. Stepanovsky, M. Yakes, V. Yeh, M. Hupalo, and M. C. Tringides, Surf. Sci. **600**, 1417 (2006).